


# SCIENTIFIC REPORTS



OPEN

## Reduced cell size, chromosomal aberration and altered proliferation rates are characteristics and confounding factors in the *STHdh* cell model of Huntington disease

Elisabeth Singer<sup>1,2</sup>, Carolin Walter<sup>1,2</sup>, Jonasz J. Weber<sup>1,2</sup>, Ann-Christin Krahl<sup>3</sup>, Ulrike A. Mau-Holzmann<sup>1</sup>, Nadine Rischert<sup>1,2</sup>, Olaf Riess<sup>1,2</sup>, Laura E. Clemensson<sup>1,2</sup> & Huu P. Nguyen <sup>1,2</sup>

Huntington disease is a fatal neurodegenerative disorder caused by a CAG repeat expansion in the gene encoding the huntingtin protein. Expression of the mutant protein disrupts various intracellular pathways and impairs overall cell function. In particular striatal neurons seem to be most vulnerable to mutant huntingtin-related changes. A well-known and commonly used model to study molecular aspects of Huntington disease are the striatum-derived *STHdh* cell lines generated from wild type and *huntingtin* knock-in mouse embryos. However, obvious morphological differences between wild type and mutant cell lines exist, which have rarely been described and might not have always been considered when designing experiments or interpreting results. Here, we demonstrate that *STHdh* cell lines display differences in cell size, proliferation rate and chromosomal content. While the chromosomal divergence is considered to be a result of the cells' tumour characteristics, differences in size and proliferation, however, were confirmed in a second non-immortalized Huntington disease cell model. Importantly, our results further suggest that the reported phenotypes can confound other study outcomes and lead to false conclusions. Thus, careful experimental design and data analysis are advised when using these cell models.

Huntington disease (HD) is an inherited, fatal, neurodegenerative disorder. It results from a CAG repeat expansion in the gene *HTT*, coding for the huntingtin protein. The mutation is translated into an elongated polyglutamine repeat in huntingtin, which leads to the disruption of various cellular signalling pathways and results in impaired cell function and ultimately cell death, particularly of striatal neurons<sup>1,2</sup>. To study cellular and molecular mechanisms contributing to the HD pathogenesis, numerous cell and animal models have been generated. The *STHdh* cell lines were generated from an HD knock-in mouse model<sup>3</sup>, which carries the endogenous *Hdh* gene (mouse Huntington disease gene homolog) with a chimeric exon 1<sup>4</sup> and is characterized by a mild behavioural phenotype and neuropathological features<sup>5</sup>. These cell lines derive from striatal primordia<sup>3</sup> and express wild-type and mutant huntingtin at endogenous levels<sup>6</sup>. The precise genetic context and the striatal origin of the cells make the *STHdh* cell lines a widely used model in HD research. By comparing immortalized striatal precursor cells from wild type mice (*STHdh*<sup>Q7/Q7</sup> cells) to precursor cells derived from heterozygous and homozygous *Hdh*<sup>Q111</sup> knock-in mice (*STHdh*<sup>Q7/Q111</sup> and *STHdh*<sup>Q111/Q111</sup> cells), differences in a variety of HD-related cellular pathways have been discovered or confirmed, for instance an involvement of huntingtin in calcium handling deficits and mitochondrial dysfunction<sup>7–11</sup> or effects on various signalling cascades<sup>12–14</sup>. Despite the to date unquestioned usefulness and importance of this model, obvious but rarely reported differences in size<sup>11</sup>, shape<sup>15</sup> and proliferation

<sup>1</sup>Institute of Medical Genetics and Applied Genomics, University of Tuebingen, 72076, Tuebingen, Germany. <sup>2</sup>Centre for Rare Diseases, University of Tuebingen, 72076, Tuebingen, Germany. <sup>3</sup>Paediatric Haematology and Oncology, University Children's Hospital Tuebingen, 72076, Tuebingen, Germany. Elisabeth Singer, Carolin Walter, Jonasz J. Weber, Laura E. Clemensson and Huu P. Nguyen contributed equally to this work. Correspondence and requests for materials should be addressed to H.P.N. (email: [hoa.nguyen@med.uni-tuebingen.de](mailto:hoa.nguyen@med.uni-tuebingen.de))

rate might demand caution when using the *STHdh* cell lines. The origin of these differences, their importance for HD, as well as the consequences for the interpretation of study outcomes remains largely unaddressed.

In this study, we show that the *STHdh* cell lines exhibit divergent characteristics, which interfere with commonly used assays and hamper the direct comparison of both cell lines. We further show that these features are partially shared by mouse embryonic fibroblast (*MEFHdh*) cell lines generated from the same animal model and their wild type littermates, which implies a common, HD-related mechanism beyond immortalization artefacts. Overall, these findings argue for a thorough characterization of every cell line used and the inclusion of such confounding factors in the experimental design.

## Results

**Reduced cell size is a characteristic of *STHdh*<sup>Q111/Q111</sup> and *MEFHdh*<sup>Q111/Q111</sup> cells.** We performed a morphometric analysis of homozygous *STHdh*<sup>Q111/Q111</sup> (STQ111) and wild type *STHdh*<sup>Q7/Q7</sup> (STQ7) cells by light microscopy and flow cytometry analysis. Measurement of the surface area of cells attached to the culture dish revealed a significantly smaller cell surface area in the mutant *STHdh* cells (Fig. 1a and b;  $P < 0.001$ ). The smaller cell size of *STHdh*<sup>Q111/Q111</sup> was also found in detached cells, both when measuring the surface area from microscopic images (Supplementary Fig. S1) and on a larger scale by flow cytometry analysis (Fig. 1c and d). Here, the relative mean forward-scatter area (FSC-A), which is positively related to cell size, was 32% lower in *STHdh*<sup>Q111/Q111</sup> than in *STHdh*<sup>Q7/Q7</sup> cells (Fig. 1d;  $P = 0.013$ ). Similar differences were also observed after differentiation into neuron-like cells (Supplementary Fig. S2).

To assess whether this cell size phenotype is cell line-specific or whether it might be considered a general feature of HD, we performed the same set of experiments in a fibroblast cell line established from the same mouse model (*MEFHdh* cells). Like in the *STHdh* cells, the mutant *MEFHdh*<sup>Q111/Q111</sup> (*MEFQ111*) cells had a smaller cell surface area compared to the wild type *MEFHdh*<sup>Q7/Q7</sup> (*MEFQ7*) cells, when the cells were attached to the culture dish (Fig. 1f;  $P = 0.03$ ). Although the difference did not reach statistical significance when manually analysing cell surface area in detached cells (Supplementary Fig. S1;  $P = 0.13$ ), it was detected again via flow cytometry analysis (Fig. 1g and h;  $P = 0.002$ ). The relative mean FSC-A of *MEFHdh*<sup>Q111/Q111</sup> cells was 31% lower compared to *MEFHdh*<sup>Q7/Q7</sup> cells, comparable to the values retrieved for *STHdh* cells (Fig. 1h). Flow cytometry analysis further revealed a higher heterogeneity of the *MEFHdh* cell population compared to *STHdh* cells, as represented by a broader distribution of cell sizes and two distinct peaks in the FSC-A plot (Fig. 1g), possibly due to the biological origin of these cell lines<sup>16</sup>.

***STHdh* but not *MEFHdh* cells show considerable chromosomal abnormalities.** As changes in DNA content can lead to alterations in cell size<sup>17,18</sup> and are a common feature of cell line stabilization<sup>19</sup> and cell passaging<sup>20,21</sup>, we performed a karyotype analysis to clarify whether the cell size differences observed in both cell lines are explained by changes in ploidy.

Karyotyping revealed a variety of chromosomal abnormalities in *STHdh* cells. Even more importantly, the chromosomal changes differed between *STHdh*<sup>Q111/Q111</sup> and *STHdh*<sup>Q7/Q7</sup> cells in qualitative and quantitative terms (Fig. 2a and b). In detail, *STHdh*<sup>Q7/Q7</sup> cells showed a hyperpentaploid, female, murine karyotype with chromosome numbers between 104 and 115. Different numerical anomalies as well as a variable number of additional, structurally abnormal chromosomes (three to eight marker chromosomes) were detected. About 40% of the cells showed at least one, but up to four additional copies of chromosome 3, 8, 9, 10, 14, 16 and 17. Interestingly, nearly 100% of the analysed cells showed two to six additional copies of chromosome 15, 18 and 19. Loss of at least one, but up to four copies was found for chromosome 4, 6, 7, 11, 12 and 13 in 40% of the cells. In contrast, *STHdh*<sup>Q111/Q111</sup> cells showed a hypo- to hypertetraploid, female, murine karyotype (77–82 chromosomes) with a high number (seven to nine) of marker chromosomes. Loss of one to four copies was found for chromosome 1, 4, 6, 7, 12, 14 and 18 - similar to *STHdh*<sup>Q7/Q7</sup> cells. Nearly all cells had one to three additional copies of chromosome 15 and 19. The total number of chromosomes was significantly lower in *STHdh*<sup>Q111/Q111</sup> cells compared to *STHdh*<sup>Q7/Q7</sup> cells (Fig. 2c;  $P < 0.001$ ).

In contrast, *MEFHdh* cells did not show marked chromosomal abnormalities (Fig. 2d and e). In detail, *MEFHdh*<sup>Q7/Q7</sup> cells showed a mainly diploid, murine, male karyotype with only some tetraploid cells (Fig. 2d). Apart from a small number of single cell anomalies, no chromosomal losses were detected. A few cells showed additional copies of chromosome 16 and 17. *MEFHdh*<sup>Q111/Q111</sup> cells showed a mainly diploid, female, murine karyotype and only a few tetraploid cells (Fig. 2e). Nearly all cells showed a numerically normal karyotype. About 50% of the cells were found to have an additional chromosome 17. The total number of chromosomes did not differ between *MEFHdh*<sup>Q111/Q111</sup> and *MEFHdh*<sup>Q7/Q7</sup> cells (Fig. 2f).

***STHdh*<sup>Q111/Q111</sup> and *MEFHdh*<sup>Q111/Q111</sup> cells show a higher proliferation rate.** We further examined the proliferation rate of *STHdh* and *MEFHdh* cells, as both mutant cell lines appeared to proliferate at different rates during regular passaging.

Quantification of the increase in cell number after 3 days of cultivation revealed an elevated proliferation rate of *STHdh*<sup>Q111/Q111</sup> compared to *STHdh*<sup>Q7/Q7</sup> cells (Fig. 3a,  $P = 0.02$ ). A trend towards increased proliferation rate was detected in *MEFHdh*<sup>Q111/Q111</sup> compared to *MEFHdh*<sup>Q7/Q7</sup> cells after 7 days of cultivation (Fig. 3b;  $P = 0.073$ ), although both *MEFHdh* cell lines did not proliferate as much as *STHdh* cells.

In order to clarify whether the enhanced proliferation had been the result of increased cell division or reduced cell death, we performed a cell cycle analysis and measured the amount of viable and apoptotic cells.

First, the proportion of cells in the different phases of the cell cycle was analysed by measuring the DNA content via DAPI staining intensity in detached, fixed cells. This assay confirmed the difference in ploidy between *STHdh*<sup>Q7/Q7</sup> and *STHdh*<sup>Q111/Q111</sup> cells, as there was a noticeable right shift in the curve obtained for *STHdh*<sup>Q7/Q7</sup>

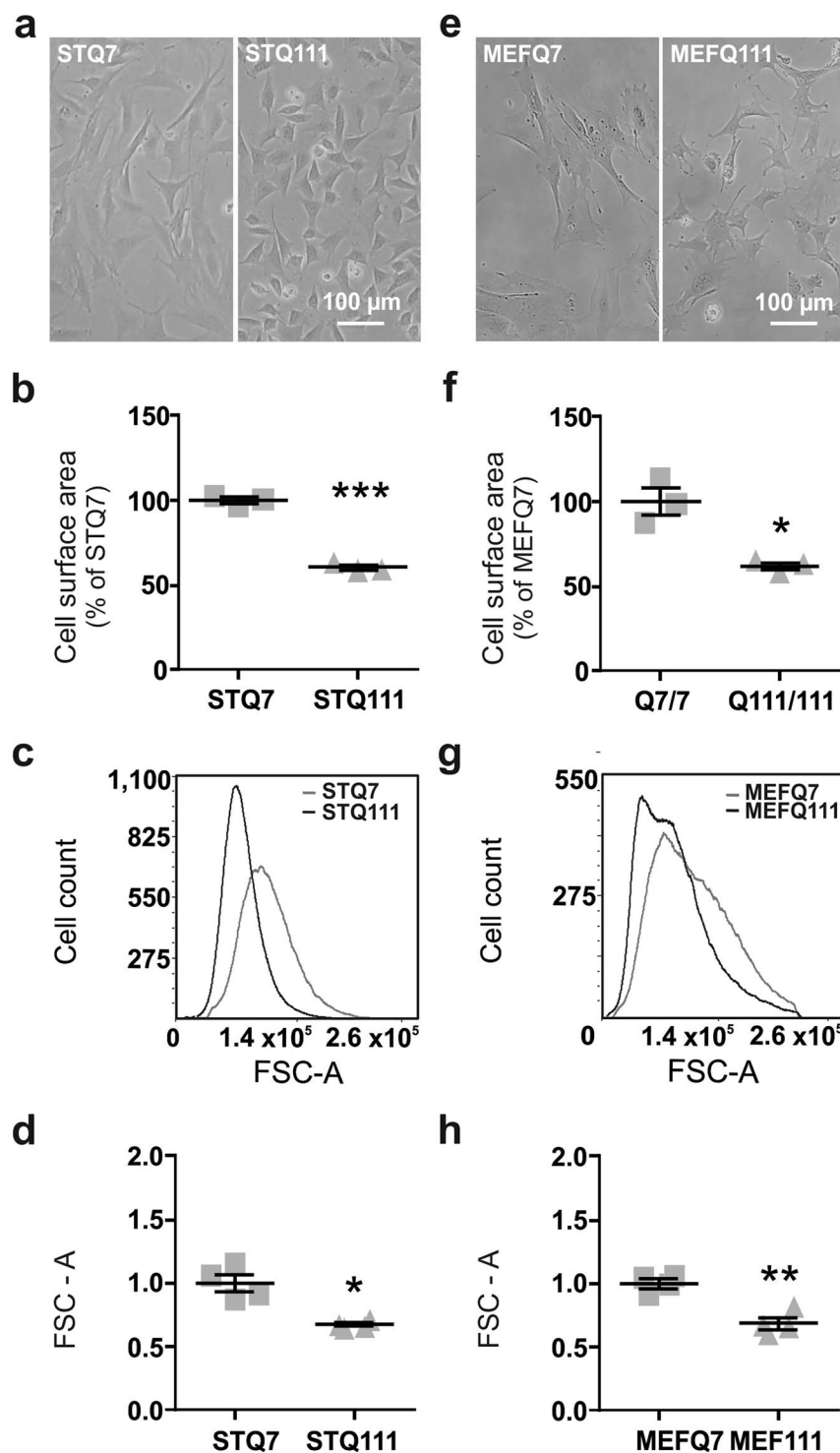


**Figure 1.** Cell size difference in Q111 knock-in cells. (a) Representative pictures of *STHdh*<sup>Q7/Q7</sup> (STQ7) and *STHdh*<sup>Q111/Q111</sup> (STQ111) cells, and (b) ImageJ-based surface area quantification of *STHdh* cells attached to the culture dish surface n = 3 experiments, unpaired *t*-tests; \*\*\**P* < 0.001. (c) Representative histograms of *STHdh* cells and (d) quantification of the cell size of live cells in suspension, based on the relative mean forward scatter area (FSC-A); n = 4 experiments, unpaired *t*-tests; \**P* < 0.05. (e–h) Results of size determination for *MEFHdh*<sup>Q7/Q7</sup> (MEFQ7) and *MEFHdh*<sup>Q111/Q111</sup> (MEFQ111) cells, respectively; \**P* < 0.05, \*\**P* < 0.01.

cells, corresponding to an overall increased DNA content (Fig. 3c). This shift, however, made the automated analysis by the analysis software unreliable, and was therefore not quantified. *MEFHdh* cells, on the other hand and in line with their similar karyograms, exhibited similar distribution patterns of cell populations with different DNA

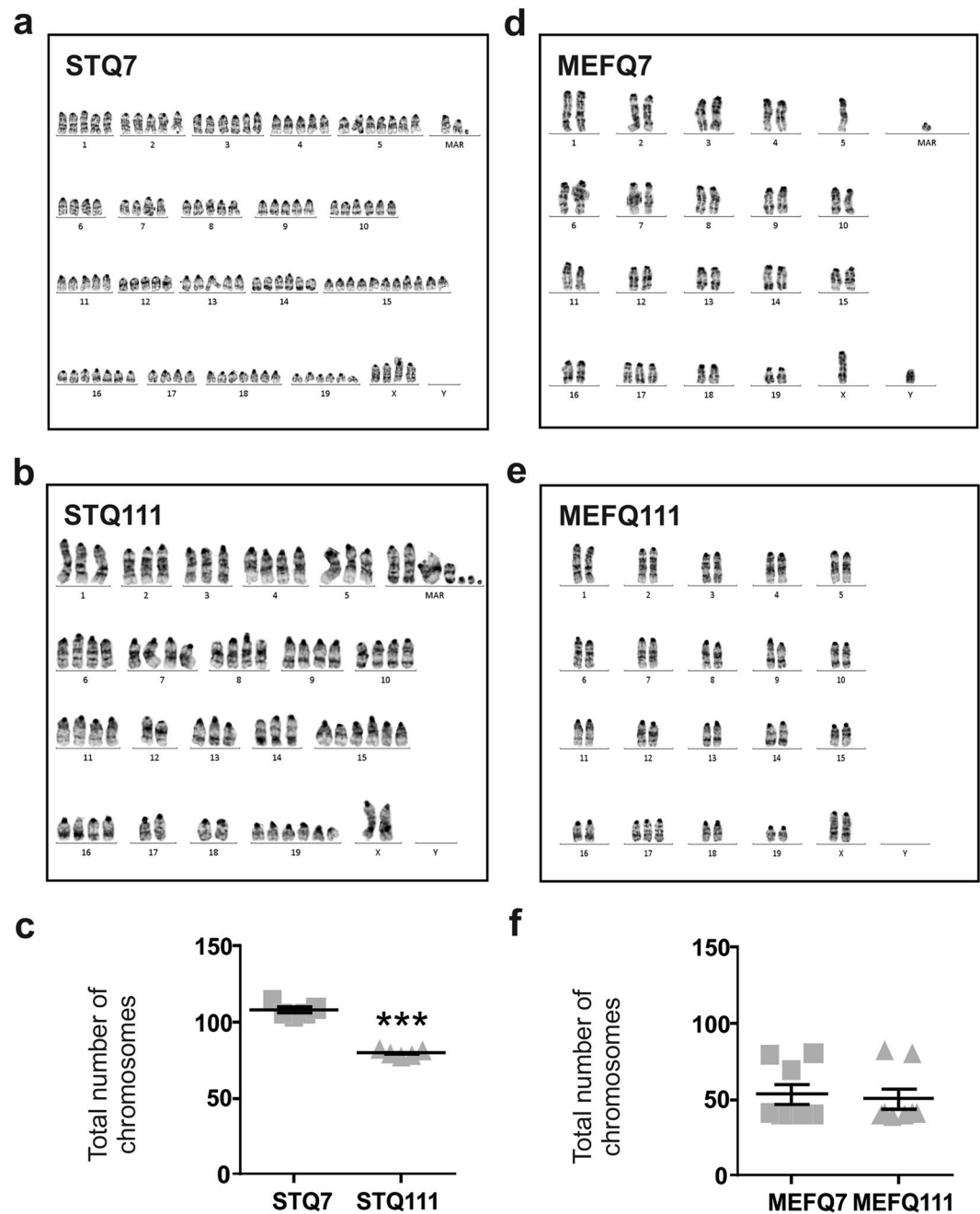


**Figure 2.** *STHdh* cells display marked and divergent chromosome abnormalities. (a) Representative karyograms from *STHdh*<sup>Q7/Q7</sup> (STQ7) and (b) *STHdh*<sup>Q111/Q111</sup> (STQ111) cells with (c) quantification of the chromosome numbers; n = 5 experiments, unpaired *t*-tests; \*\*\**P* < 0.001. (d–f) Result of karyogram analysis for *MEFHdh*<sup>Q7/Q7</sup> (MEFQ7) and *MEFHdh*<sup>Q111/Q111</sup> (MEFQ111) cells, respectively; n = 8 experiments.

content (Fig. 3d). In this case, the analysis showed a significant decrease in cells in the G<sub>0</sub>/G<sub>1</sub> phase (*MEFHdh*<sup>Q7/Q7</sup> 65.73 ± 2; *MEFHdh*<sup>Q111/Q111</sup> 39.17 ± 1; *P* = 0.0003), alongside a tendency to an increase in cells in the S (*MEFHdh*<sup>Q7/Q7</sup> 4.1 ± 2; *MEFHdh*<sup>Q111/Q111</sup> 8.2 ± 0.2; *P* = 0.07) and G<sub>2</sub>/M phase (*MEFHdh*<sup>Q7/Q7</sup> 22.9 ± 4; *MEFHdh*<sup>Q111/Q111</sup> 38.1 ± 0.2; *P* = 0.03). The observed differences in cell cycle progression were in line with the observation that *MEFHdh* cells containing the *huntingtin* knock-in mutation proliferate more than wild type cells.

Second, we analysed the amount of viable and apoptotic cells by flow cytometry analysis (Fig. 4). We found *STHdh*<sup>Q111/Q111</sup> cells to have a higher proportion of viable cells (Fig. 4b, *P* = 0.047), and in turn a lower proportion of apoptotic cells compared to *STHdh*<sup>Q7/Q7</sup> cells, although the latter did not reach statistical significance. Similar results were obtained for *MEFHdh* cells, showing a significantly higher proportion of viable cells (Fig. 4e; *P* = 0.026) and, in this case, a significantly lower number of apoptotic cells (Fig. 4f; *P* = 0.017) in *MEFHdh*<sup>Q111/Q111</sup> cells compared to their wild type control.

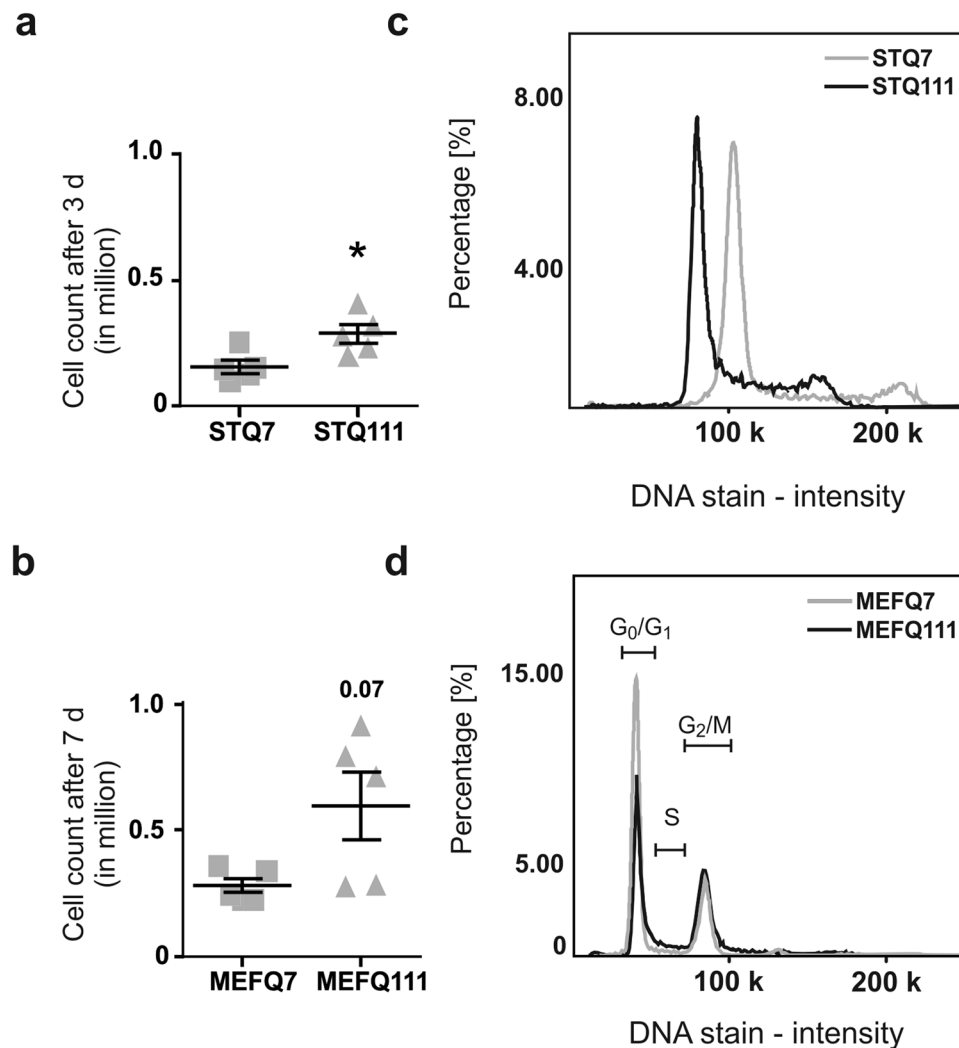


**Figure 3.** Both mutant cell lines exhibit increased proliferation rates. (a) Manually determined cell count of *STHdh* cells after 3 days;  $n = 5$  experiments, unpaired  $t$ -tests;  $*P < 0.05$  and (b) manually determined cell count of *MEFHdh* cells after 7 days;  $n = 5$  experiments, unpaired  $t$ -tests. (c) Representative overlays of signal intensity of *STHdh*<sup>Q7/Q7</sup> and *STHdh*<sup>Q111/Q111</sup> DAPI-stained cells and (d) representative overlay of signal intensity of *MEFHdh*<sup>Q7/Q7</sup> and *MEFHdh*<sup>Q111/Q111</sup> DAPI-stained cells with exemplary indication of cell cycle;  $n = 3$ .

#### The cell size and proliferation phenotypes in *STHdh*<sup>Q111/Q111</sup> cells might impede the interpretation of standard cell viability assays.

When investigating cell viability in our study, we used flow cytometry, a method that should theoretically be independent of cell size and cell proliferation. However, common cell viability tests depend considerably on these parameters. Thus, we reassessed cell viability and cell death using the standard cell viability assays, PrestoBlue<sup>®</sup> and LDH assay, respectively (Fig. 5).

Analysis of the data revealed contradicting results when compared to the outcomes from flow cytometry. The PrestoBlue<sup>®</sup> assay consistently showed lower signals in *STHdh*<sup>Q111/Q111</sup> cells (Fig. 5a;  $P = 0.031$ ) and the LDH assay revealed increased LDH release in *STHdh*<sup>Q111/Q111</sup> compared to *STHdh*<sup>Q7/Q7</sup> cells (Fig. 5b;  $P = 0.022$ ), suggesting that mutant cells are characterized by reduced viability and increased cell death, in contrast to the first findings. Differentiation of *STHdh* cells led to a similar readout as flow cytometry (Supplementary Fig. S3).

The results obtained for *MEFHdh* cells differed from the results obtained for *STHdh* cells. *MEFHdh*<sup>Q111/Q111</sup> cells had similar signals as *MEFHdh*<sup>Q7/Q7</sup> cells in the PrestoBlue<sup>®</sup> assay (Fig. 5c;  $P = 0.656$ ), but showed reduced LDH release (Fig. 5d;  $P = 0.034$ ). These findings were comparable to the results obtained by flow cytometry.

#### Chromosomal abnormalities in *STHdh*<sup>Q111/Q111</sup> cells might impede the interpretation of western blot analyses.

Since we observed that *STHdh*<sup>Q111/Q111</sup> cells differ markedly from the control *STHdh*<sup>Q7/Q7</sup> cell line in terms of chromosomal constitution, we investigated possible consequences of these alterations on the protein levels of commonly used loading controls for western blot analysis. The four proteins,  $\beta$ -actin (*Actb*, chromosome 5), GAPDH (*Gapdh*, chromosome 6),  $\alpha$ -tubulin (*Tuba1a*, chromosome 15) and vinculin (*Vcl*, chromosome 14) are located on different chromosomes.

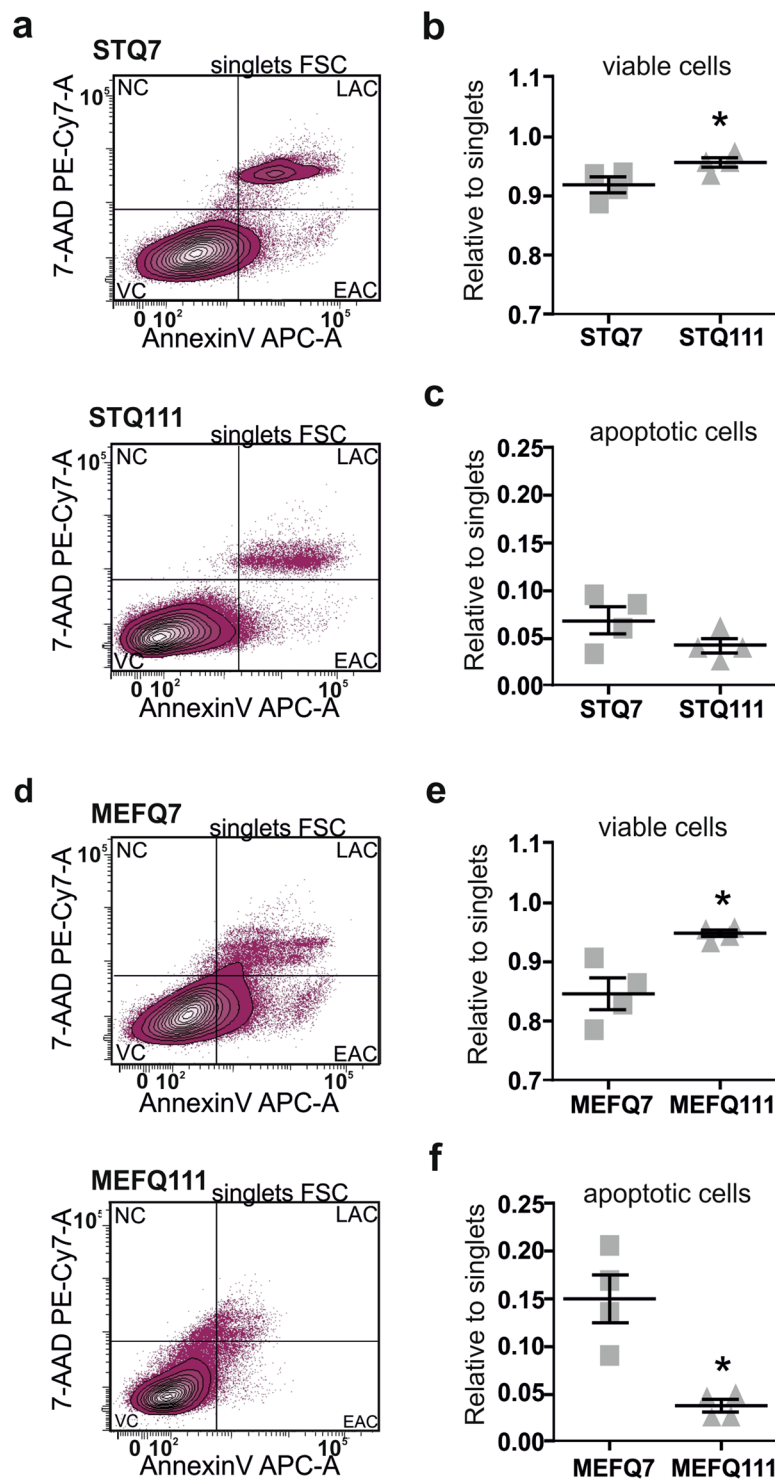


**Figure 4.** Cell viability is not reduced in *STHdh* and *MEFHdh* mutant cell lines. Results from cell size- and cell number-independent flow cytometry analysis: **(a)** Representative scatterplots of flow cytometry analysis of *STHdh* cells and **(b and c)** quantification from flow cytometry analysis of Annexin V/7'AAD staining;  $n = 4$  experiments. VC: viable cells, EAC: early apoptotic cells, LAC: late apoptotic cells, NC: necrotic cells. Quantification of apoptotic cells combines results for EAC and LAC; unpaired  $t$ -tests; \* $P < 0.05$ . **(d–f)** Results of *MEFHdh* cells, respectively; unpaired  $t$ -tests; \* $P < 0.05$ .

Western blot analysis of RIPA cell lysates revealed strong trends toward decreased levels of  $\alpha$ -tubulin and vinculin in *STHdh*<sup>Q111/Q111</sup> cells compared to *STHdh*<sup>Q7/Q7</sup> cells (Fig. 6b and c;  $P = 0.06$ ,  $P = 0.03$ ), in accordance with the reduced number of chromosomes 15 and 14 in *STHdh*<sup>Q111/Q111</sup> cells. In contrast, these differences were

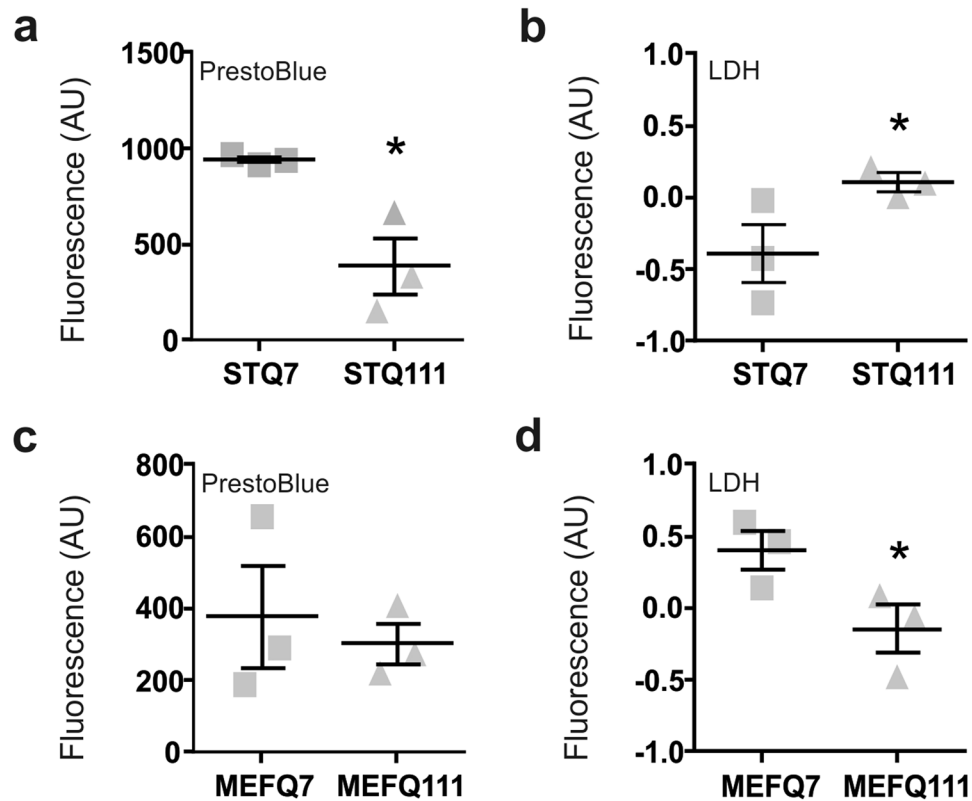


**Figure 5.** The cell size and proliferation phenotypes in *STHdh*<sup>Q111/Q111</sup> cells impede the interpretation of standard cell viability assays. Results from the cell size- and cell number-dependent tests for *STHdh* cells: (a) PrestoBlue®, n = 3 experiments and (b) LDH assay, n = 3 experiments. Unpaired *t*-tests; \**P* < 0.05. (c and d) Results from size- and cell number-dependent tests for *MEFHdh* cells, respectively; unpaired *t*-tests; \**P* < 0.05.

not found in *MEFHdh* cells (Fig. 6e and f), where no differences in the number of chromosomes 15 and 14 were detected. Furthermore, the levels of  $\beta$ -actin were comparable in *STHdh*<sup>Q111/Q111</sup> and *STHdh*<sup>Q7/Q7</sup> cells (Fig. 6b and c) as well as in *MEFHdh*<sup>Q111/Q111</sup> and *MEFHdh*<sup>Q7/Q7</sup> cells (Fig. 6e and f), in accordance with the similar numbers of chromosome 5 in mutant and control cell lines. Interestingly, despite equal numbers of chromosome 6, levels of GAPDH were elevated in *STHdh*<sup>Q111/Q111</sup> and tendentially in *MEFHdh*<sup>Q111/Q111</sup> cell lines, compared to their wild type counterparts (Fig. 6b,c; *P* = 0.06, e and f; *P* = 0.02).

## Discussion

*STHdh* cells represent a widely used cell culture model for studying cellular and molecular aspects of HD. Differences in cell morphology, growth and differentiation have previously been mentioned by other groups<sup>15,22</sup>, but to date, these differences have not been assessed quantitatively. Our study demonstrates clear differences in cell size, proliferation and ploidy between mutant and wild type *STHdh* cells, and suggests a strong influence of these phenotypes on other readouts.

In the first description of the *STHdh* cell lines, it was stated that *STHdh*<sup>Q111/Q111</sup> cells are of similar size as *STHdh*<sup>Q7/Q7</sup> cells, while cell proliferation was even decreased in the mutant cells and accompanied by an increase in DNA content<sup>3</sup>. Later studies, however, either do mention a reduced cell size of *STHdh*<sup>Q111/Q111</sup> cells<sup>11,15</sup>, or the results are at least suggestive of such a phenotype (although not specifically discussed in these papers)<sup>23–25</sup>. This might indicate that the phenotypes observed in our study had developed over time, possibly due to the tumour character of the cell lines. On the other hand, a reduced cell size was also found in our *MEFHdh*<sup>Q111/Q111</sup> cell line compared to the respective control, despite the absence of large scale chromosomal changes. In addition, cell size differences in striatal neurons have been reported for the R6/2 model<sup>26,27</sup> and the YAC128 model<sup>28</sup>, two transgenic mouse models of HD, and it has been suspected for HD patients<sup>29</sup>. It remains uncertain, if the reduced cell size should be considered an artefact or could be an HD-related feature, although it might be concluded that huntingtin is at least somehow involved in cell size regulation, as it is, as well, known to interact with cytoskeletal proteins<sup>30</sup>.

The multiple numerical anomalies and structurally abnormal chromosomes we found in both *STHdh* cell lines are typical for stable cell lines and long-term passaging<sup>19–21</sup>. Importantly, these abnormalities were found in cell populations that had been passaged for a maximum of six times between their purchase and the respective karyogram analysis. As this is a normal amount of passages required to carry out experiments, the abnormalities are likely to appear in other laboratories in a similar magnitude. Thus, users should be aware that the cell lines might not show the characteristics according to the original publication.

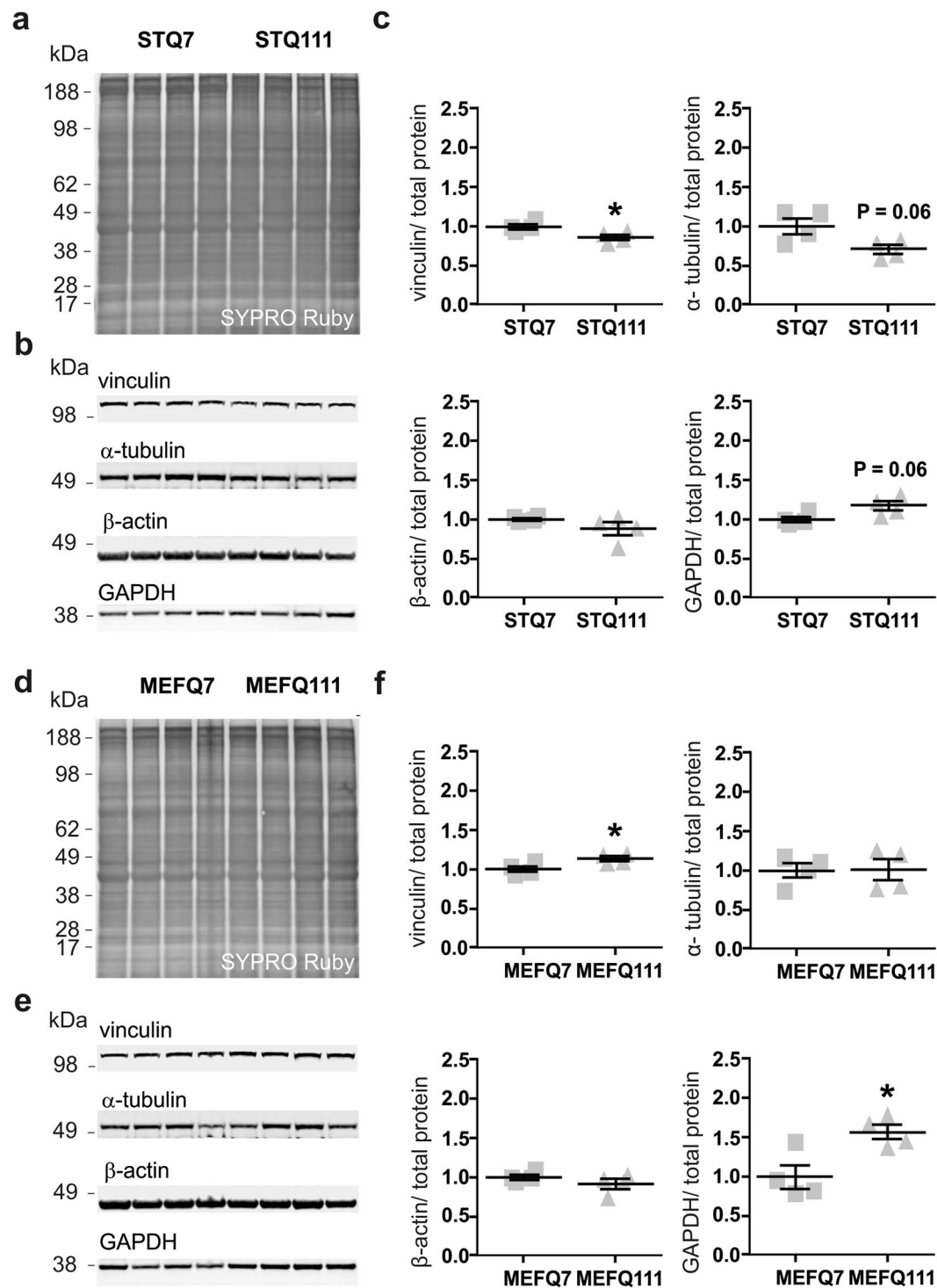


**Figure 6.** Chromosomal abnormalities impede the interpretation of western blot results in *STHdh* cells. (a) SYPRO Ruby staining, (b) western blots and (c) corresponding quantification of marker proteins in *STHdh* cells. Unpaired *t*-tests; \* $P < 0.05$ . (d) SYPRO Ruby staining, (e) western blots and (f) corresponding quantification of marker proteins in *MEFHdh* cells. Unpaired *t*-tests; \* $P < 0.05$ .

We further found the *STHdh*<sup>Q111/Q111</sup> as well as *MEFHdh*<sup>Q111/Q111</sup> cells to have an increased proliferation rate. It had been reported earlier that mutant huntingtin is involved in cell division in cell models and *Drosophila*<sup>31</sup>, as well as *Hdh*<sup>Q111/111</sup> knock-in mice, *STHdh*<sup>Q111/Q111</sup> cells and *MEFHdh*<sup>Q111/Q111</sup> cells, as it alters the orientation of the mitotic spindle<sup>32</sup>. Although cell proliferation had not been measured in that study, the authors demonstrate that this leads to changes in neurogenesis in the developing cortex, highlighting the importance of this phenotype.

It is perceivable that differences in cell size, proliferation rate and chromosomal content might constitute confounding factors, and might complicate the interpretation of study outcomes due to adding several variables



which cannot properly be controlled for. We demonstrated that assays based on cell size and number, such as the PrestoBlue<sup>®</sup> and LDH assay, revealed lower basal cell viability and increased cell mortality in *STHdh*<sup>Q111/Q111</sup> cells. Similar results have previously been published by others using the same assays<sup>33–35</sup> or comparable methods<sup>7</sup>. However, the results could not be recreated in an assay that was likely to not depend on cell size or cell number. Thus, the earlier reported baseline difference in cell viability between *STHdh*<sup>Q111/Q111</sup> and *STHdh*<sup>Q7/Q7</sup> cells is questionable. Interestingly, our results were even indicative of increased cell viability in both, *STHdh*<sup>Q111/Q111</sup> and *MEFHdh*<sup>Q111/Q111</sup>. Effects on pro-survival functions in *STHdh*<sup>Q111/Q111</sup> cells would need to be further investigated, as they have been reported to be reduced for other cell models of HD<sup>36,37</sup>, whereas Akt signalling, implicated in neuronal survival<sup>38</sup>, has been shown to be increased in mutant *STHdh* cells<sup>14</sup>. Clearly, *STHdh* cells do not represent the hallmarks of the advanced disease. Intranuclear inclusions, amongst others, found in *in vitro* and *in vivo* models, are not found in *STHdh* cells<sup>3</sup>. Therefore, the disease stage they model might not necessarily be characterized by a reduction in cell viability under normal conditions.

Confounding effects of the chromosomal abnormalities found in the *STHdh* cell lines were further expected for western blot analyses. Our investigations revealed important aspects to be considered when choosing a loading control for western blot analysis in *STHdh* cells. The protein levels of  $\alpha$ -tubulin and vinculin were lower in *STHdh*<sup>Q111/Q111</sup>, but not in *MEFHdh*<sup>Q111/Q111</sup>, when compared to their respective controls and can be interpreted as a direct effect of the lower copy number of the chromosomes 14 and 15 in the *STHdh*<sup>Q111/Q111</sup> cells. These observations correspond to previous studies, which reported on analogous proteomic changes resulting from variations of the gene copy number in cancer cells or aneuploid cell lines<sup>39,40</sup>. On the other hand, our observation of an elevated GAPDH expression in both *STHdh*<sup>Q111/Q111</sup> and *MEFHdh*<sup>Q111/Q111</sup> cells has already been shown in other HD models. As GAPDH is a well-known interaction partner of huntingtin, these results further render GAPDH as an inadequate loading control in HD research<sup>41–43</sup>.

Although our study is important, as it demonstrates features of the extensively used *STHdh* model that need to be considered when working with this cell model, and as it highlights the *MEFHdh* cells as useful controls in *in vitro* studies, there are some limitations that we would like to point out. First, our *MEFHdh* cells were generated from embryos of different sex. The *MEFHdh* cells were generated 12 days after a 48-hour breeding period, and sex differentiation in the mouse embryo begins as early as E10<sup>44</sup>. Therefore, although we consider the influence of sex determination on cell size, proliferation rate and chromosomal content at that point negligible, we cannot rule it out. Thus, we highly recommend the generation of sex-matched *MEFHdh* cell lines for further studies. Second, the two cell lines characterized here originate from the same HD animal model. As such, they share several drawbacks that need to be considered. *Hdh*<sup>Q111</sup> knock-in mice, like most other animal models of HD, are designed to express mutant huntingtin with high numbers of polyglutamine repeats to provoke possibly early and strong phenotypes (reviewed by Ferrante *et al.*<sup>45</sup>), even though such high repeat numbers are only found in patients with the rare juvenile form of HD. In this regard, it should be noted that cell models<sup>46</sup> and animal models<sup>47</sup> with lower CAG-repeats have been generated to recapitulate the commonly found mutation lengths. Furthermore, both *STHdh* and *MEFHdh* cell lines are not isogenic. Q7 alleles represent the wild type mouse alleles, while Q111 alleles are human mouse chimera of exon 1. For this reason, there are additional differences in the gene sequence between Q7 and Q111 alleles than the CAG repeat expansion. On the other hand, *STHdh* and *MEFHdh* cells differ fundamentally regarding immortalization and biological origin. *STHdh* cells are comparable to other immortalized cell lines with regard to immortalization artefacts<sup>19–21,48</sup>, as shown here by the altered chromosome numbers. This is a drawback, as the supposedly complementary Q7 and Q111 cell lines have apparently acquired divergent features over time. Moreover, it needs to be considered that p53, a tumour suppressor protein affected in immortalized cell lines<sup>49,50</sup>, is a transcriptional regulator of *huntingtin*<sup>51</sup> and implicated in the pathogenesis of HD<sup>52</sup>. In this regard, the *MEFHdh* cells used here represent a better cell model, as these were not immortalized and therefore the genetic integrity was less corrupted. However, the *MEFHdh* cells presented milder phenotypes regarding cell size and proliferation, which is likely to be due to their heterogeneous cell composition<sup>16</sup>. In this regard, the clonal and neuronal character of *STHdh* cells might lead to stronger and more robust phenotypes than embryonic fibroblasts. The clonal character, however, once more underscores the importance of an additional model, to exclude artefacts. Finally, it would always be advantageous to confirm phenotypes in cell and animal models of HD that are based on a different genetic background.

In summary, *STHdh* cell lines are a generally useful model to study mechanisms behind the molecular pathogenesis of HD, because they provide the proper cellular as well as genetic context of HD due to their striatal origin and the knock-in model they derive from. However, the possible bias due to differences in cell size, proliferation and chromosomal content need to be considered when planning and interpreting results. In this regard, assays in which cell size and cell number play an important role for the outcome, and cannot be controlled for, should be avoided. Differentiation of the *STHdh* cells into neuron-like cells might at least overcome the problem regarding cell proliferation. Nevertheless, for time-course experiments the increased proliferation rate, as it was, as well, observed in *MEFHdh* cells needs to be considered. A simple solution for treatment studies would be to not directly compare results from *STHdh*<sup>Q7/Q7</sup> to *STHdh*<sup>Q111/Q111</sup>, but to rather compare treatment effects in the two cell lines independently. Finally, using a second *in vitro* or an *in vivo* model to confirm results is beneficial to determine the HD-dependency of the phenotype investigated. Our study emphasizes that it is of importance to regularly check the basic characteristics of an employed cell model and to consider putative alterations for experimental design and analysis.

## Methods

**Ethics Statement.** Experiments for the generation of *MEFHdh* cells were performed at the University of Tuebingen. The protocol was approved by the local ethics committee at Regierungspraesidium Tuebingen and carried out in accordance with the German Animal Welfare Act and the guidelines of the Federation of European Laboratory Animal Science Associations, based on European Union legislation (Directive 2010/63/EU).

**STHdh cells.** *STHdh* cell lines, originally generated at the laboratory of Dr. Marcy MacDonald (Harvard Medical School, Boston)<sup>3</sup>, were purchased from Coriell Cell Repositories (Coriell Institute for Medical Research). Cell passages 4–12 were used for the experiments.

**MEFHdh cells.** A heterozygous breeding of *Hdh*<sup>Q111</sup> knock-in mice was set up and maintained for 48 hours. After 12 days, the pregnant female was sacrificed by inhalation of CO<sub>2</sub>. The embryos were extracted by caesarean sectioning, decapitated immediately and placed individually in sterile, ice-cold, Dulbecco's phosphate-buffered saline (DPBS) (Invitrogen). Limbs, brain and visceral organs were removed. The remaining tissue was transferred into a sterile well of a 6-well plate with fresh DPBS, which was then replaced by 2 ml of culture media (Dulbecco's Modified Eagle Medium (DMEM) with 1% penicillin/streptomycin and 10% fetal calf serum (FCS), Gibco®, Thermo Fisher Scientific). The tissue was incubated for 1 h at 37 °C and 5% CO<sub>2</sub>. After this, the tissue was transferred into a 100 mm dish with 10 ml culture media (pre-warmed to 37 °C), and minced with a scalpel. Pieces were transferred to a T75 cell culture flask with 10 ml of fresh media and incubated at 37 °C and 5% CO<sub>2</sub> for 3 days. Afterwards, media was changed and the cells were incubated until they reached 90% confluency. Cells were then trypsinized (1 ml 0.25% trypsin-EDTA (Invitrogen) for 5 min at 37 °C and 5% CO<sub>2</sub>) and gently resuspended using a 1 ml pipette for subcultivation. For the experiments, a wild type and a homozygous culture were picked.

**Cell handling and treatment.** *STHdh* and *MEFHdh* cells were maintained in DMEM supplemented with 10% FCS (Gibco™) and 1% penicillin/streptomycin (Gibco™) at 37 °C in 5% CO<sub>2</sub>. *STHdh* media was additionally complemented by adding 1% geneticin (A2912, Biochrome). Both, *STHdh* and *MEFHdh* cells were routinely tested negative for contamination by mycoplasma using the Venor®*GeM* Mycoplasma detection kit (Merck). Unless specifically stated differently, *STHdh* cells were undifferentiated. For differentiation into neuron-like cells a previously described differentiation protocol<sup>3</sup> was used. For this, cells were incubated in differentiation cocktail for 24–48 h.

**Flow cytometry.** Undifferentiated *STHdh* and *MEFHdh* cells were recorded using a flow cytometry LSR II cytofluorometer (BD Bioscience). A total of 200,000 ungated events were analysed with the flow cytometry-DIVA software version 6.1.3 (BD Bioscience) and overlays were processed with FCS Express software version 4.0.230 (De Novo Software). Differentiated *STHdh* cells were recorded with a CyAn™ ADP flow cytometer (Beckman Coulter). A total of 20,000 ungated events were analysed with Summit V4.3.01 software (Dako Colorado, Inc.).

**Cell size determination.** Cells were seeded in 6-well plates and grown to 60–70% confluency. Cell size was measured for cells attached to the surface of the culture dish as well as for detached cells after trypsinization each with 3 replicates per cell line. A total of 270 cells per genotype were analysed in 3 independent experiments (30 cells/well; 3 wells/experiment). Pictures of the cells were taken using an Eclipse TS100 Inverted Routine microscope (Nikon) with a digital camera at 20x magnification and analysed with ImageJ v1.47<sup>53</sup>. For attached cells, the area of the cells was approximated by measuring the area of a polygon that was assigned to each cell. For detached cells, the area of a round shape was measured that was applied to each cell individually. The scale was determined by the length of the counting chamber grid.

**Chromosome analysis.** Chromosome preparations from cultured cells and GTG-banding were performed using standard techniques. For each cell line, 17 mitoses were numerically analysed and 5–8 mitoses were structurally analysed. For cytogenetic analyses, for all cell lines, cells from early passages (P4–P6) were harvested using a standard protocol and was followed by G-banding. Images of well spread metaphase chromosomes were captured using a CCD camera. Karyotyping was performed using the IKAROS software (MetaSystems, Altlußheim, Germany). Chromosome classification followed the guidelines of the International Committee on Standardized Genetics nomenclature for mice<sup>54</sup>.

**Determination of proliferation rate.** Three replicates of *STHdh* (40,000 cells per well) and *MEFHdh* cells (100,000 cells per well) were seeded in 6-well plates. After 3 days (*STHdh*) or 7 days (*MEFHdh*), cells were harvested by trypsinization (250 µl 0.25% trypsin-EDTA (Gibco™) for 5 min at 37 °C and 5% CO<sub>2</sub>), washed and counted again. At least three independent experiments were performed.

**Determination of DNA content.** DNA content was measured using the NucleoView NC-3000 (ChemoMetec). Reagents were provided by the manufacturer and cells were treated according to the manufacturer's instructions. In brief, cells were detached from the culture flask, washed with DPBS (Gibco™) and lysed. The cells were stained with DAPI, at a saturating concentration (10 µg/ml), stabilized and immediately analysed with the device. Data was analysed with the NucleoView NC-3000 software, Version 2.1.25.12 (ChemoMetec).

**Viability assays.** Cell viability and cell death were determined using commercially available kits (PrestoBlue® cell viability reagent, Invitrogen™; Cytotoxicity Detection Kit (LDH), Roche), following the provider's instructions. Briefly, 10,000 cells were seeded in a 96-well plate and incubated overnight. Culture media was transferred into a new 96 well plate for the LDH assay. Cells left in the original plate received fresh media containing PrestoBlue®. The fluorescence intensity (PrestoBlue® assay) was measured after 1 h; the absorption (LDH assay) was measured according to manufacturer's instructions, using the plate reader MWGt Synergy HT (BioTek Instruments) and the software Gen5 2.01 (BioTek).

In addition, cell viability and cell death were measured using flow cytometry. For this, cells were grown in 75 ml culture flasks and harvested by gentle trypsinization (0.25% Trypsin-EDTA; Gibco®, Thermo Fisher Scientific). Cells were centrifuged at 400 × g for 5 min and washed twice with 1 × Annexin V Binding Buffer (eBioscience). Cells were labelled with Alexa Fluor® 647 Annexin V (Biolegend) and 7-Amino-Actinomycin (7'AAD) (BD Pharmingen). Data was recorded by flow cytometry to determine the number of Annexin V/7'AAD-positive cells.

**Cell lysate preparation.** For preparation of lysates, *STHdh* and *MEFHdh* cells were trypsinized and collected by centrifugation at  $350 \times g$  for 5 min. The pellet was washed once with cold DPBS (Gibco<sup>®</sup>, Thermo Fisher Scientific), centrifuged again and lysed in RIPA buffer (50 mM Tris pH 7.5, 150 mM NaCl, 0.1% SDS, 0.5% sodium deoxycholate and 1% Triton X-100, containing protease inhibitors) for 25 min on ice, while vortexing briefly every 5 min. Afterwards, samples were centrifuged at  $13,200 \times g$  for 15 min at 4 °C. Supernatant was pipetted into a pre-cooled reaction tube, adding glycerol to final concentration of 10%, and stored at –80 °C until further analysis.

**Western blotting, SYPRO Ruby staining and immunodetection.** Protein concentrations of RIPA lysates were determined spectrophotometrically using Bradford reagent (Bio-Rad Laboratories). Western blot analysis was performed following standard procedures. Briefly, 30 µg of protein were separated electrophoretically using 10% Bolt<sup>®</sup> Bis-Tris Plus Gels (Thermo Fisher Scientific). Proteins were transferred on Amersham<sup>™</sup> Protran<sup>™</sup> Premium 0.2 µm nitrocellulose membranes (GE Healthcare) using a TE22 Transfer Tank (Hoefer).

After transfer, total protein was stained with SYPRO Ruby Protein Blot Stain (Thermo Fisher Scientific) according to manufacturer's instructions and detected at 600 nm using the LI-COR ODYSSEY<sup>®</sup> FC imaging system (LI-COR Biosciences).

After SYPRO Ruby staining, membranes were blocked with 5% Slimfast in TBS at room temperature for 1 h and probed overnight at 4 °C with the following primary antibodies: mouse anti-β-actin (1:10,000; clone AC-15, A5441, Sigma Aldrich), mouse anti-GAPDH (1:1000; clone GA1R, ab125247, Abcam), mouse anti-α-tubulin (1:5000; clone DM1A, CP06, EMD Millipore) and rabbit anti-vinculin (1:1000; clone E1E9V, #13901, Cell signaling). Afterwards, membranes were incubated at room temperature for 1 h with the respective secondary IRDye antibodies goat anti-mouse 680LT and goat anti-rabbit 800CW (all 1:10,000; LI-COR Biosciences). Fluorescence signals were detected with the LI-COR ODYSSEY<sup>®</sup> FC and quantified with ODYSSEY<sup>®</sup> Server software version 4.1 (LI-COR Biosciences). Quantified signals were normalized to total protein as detected before using SYPRO Ruby Protein Stain.

**Statistical Analysis and Data availability.** All data are presented as individual measurements (grey shapes) with mean and standard error of the mean (SEM). Statistical analysis was performed with GraphPad Prism 6.00 for Windows (GraphPad Software, Inc). Statistical significance of two group data sets was determined using two-tailed, unpaired Student's *t*-test, with Welch's correction. The significance threshold was set to  $P < 0.05$ . The datasets generated during and/or analysed during the current study are available from the corresponding author on reasonable request.

## References

- Vonsattel, J. P. *et al.* Neuropathological classification of Huntington's disease. *Journal of neuropathology and experimental neurology* **44**, 559–577 (1985).
- Zuccato, C. & Cattaneo, E. Brain-derived neurotrophic factor in neurodegenerative diseases. *Nat Rev Neurol* **5**, 311–322 (2009).
- Trettel, F. *et al.* Dominant phenotypes produced by the HD mutation in *STHdh*(Q111) striatal cells. *Hum Mol Genet* **9**, 2799–2809 (2000).
- Menalled, L. B. Knock-In Mouse Models of Huntington's Disease. *NeuroRX* **2**, 465–470 (2005).
- Wheeler, V. C. *et al.* Early phenotypes that presage late-onset neurodegenerative disease allow testing of modifiers in *Hdh* CAG knock-in mice. *Human Molecular Genetics* **11**, 633–640, <https://doi.org/10.1093/hmg/11.6.633> (2002).
- Wheeler, V. C. *et al.* Long glutamine tracts cause nuclear localization of a novel form of huntingtin in medium spiny striatal neurons in *Hdh*Q92 and *Hdh*Q111 knock-in mice. *Human Molecular Genetics* **9**, 503–513, <https://doi.org/10.1093/hmg/9.4.503> (2000).
- Gines, S. *et al.* Specific progressive cAMP reduction implicates energy deficit in presymptomatic Huntington's disease knock-in mice. *Human Molecular Genetics* **12**, 497–508, <https://doi.org/10.1093/hmg/ddg046> (2003).
- Oliveira, J. M. A. *et al.* Mitochondrial-Dependent Ca<sup>2+</sup> Handling in Huntington's Disease Striatal Cells: Effect of Histone Deacetylase Inhibitors. *The Journal of Neuroscience* **26**, 11174–11186, <https://doi.org/10.1523/jneurosci.3004-06.2006> (2006).
- Choo, Y. S., Johnson, G. V., MacDonald, M., Detloff, P. J. & Lesort, M. Mutant huntingtin directly increases susceptibility of mitochondria to the calcium-induced permeability transition and cytochrome c release. *Hum Mol Genet* **13**, 1407–1420, <https://doi.org/10.1093/hmg/ddh162> (2004).
- Seong, I. S. *et al.* HD CAG repeat implicates a dominant property of huntingtin in mitochondrial energy metabolism. *Hum Mol Genet* **14**, 2871–2880, <https://doi.org/10.1093/hmg/ddi319> (2005).
- Milakovic, T. & Johnson, G. V. Mitochondrial respiration and ATP production are significantly impaired in striatal cells expressing mutant huntingtin. *J Biol Chem* **280**, 30773–30782, <https://doi.org/10.1074/jbc.M504749200> (2005).
- Xifro, X., Garcia-Martinez, J. M., Del Toro, D., Alberch, J. & Perez-Navarro, E. Calcineurin is involved in the early activation of NMDA-mediated cell death in mutant huntingtin knock-in striatal cells. *J Neurochem* **105**, 1596–1612, <https://doi.org/10.1111/j.1471-4159.2008.05252.x> (2008).
- Ferrante, A. *et al.* Expression, pharmacology and functional activity of adenosine A1 receptors in genetic models of Huntington's disease. *Neurobiol Dis* **71**, 193–204, <https://doi.org/10.1016/j.nbd.2014.08.013> (2014).
- Gines, S., Ivanova, E., Seong, I. S., Saura, C. A. & MacDonald, M. E. Enhanced Akt signaling is an early pro-survival response that reflects N-methyl-D-aspartate receptor activation in Huntington's disease knock-in striatal cells. *J Biol Chem* **278**, 50514–50522, <https://doi.org/10.1074/jbc.M309348200> (2003).
- Reis, S. A. *et al.* Striatal neurons expressing full-length mutant huntingtin exhibit decreased N-cadherin and altered neurogenesis. *Hum Mol Genet* **20**, 2344–2355, <https://doi.org/10.1093/hmg/ddr127> (2011).
- Singhal, P. K. *et al.* Mouse embryonic fibroblasts exhibit extensive developmental and phenotypic diversity. *Proc Natl Acad Sci USA* **113**, 122–127, <https://doi.org/10.1073/pnas.1522401112> (2016).
- Lee, H. O., Davidson, J. M. & Duronio, R. J. Endoreplication: polyploidy with purpose. *Genes & Development* **23**, 2461–2477, <https://doi.org/10.1101/gad.1829209> (2009).
- Gregory, T. R. Coincidence, coevolution, or causation? DNA content, cell size, and the C-value enigma. *Biological Reviews* **76**, 65–101, doi:undefined (2001).
- Stewart, N. & Bacchetti, S. Expression of SV40 large T antigen, but not small t antigen, is required for the induction of chromosomal aberrations in transformed human cells. *Virology* **180**, 49–57 (1991).

20. Gaztelumendi, N. & Nogués, C. Chromosome Instability in mouse Embryonic Stem Cells. *Scientific Reports* **4**, 5324, <https://doi.org/10.1038/srep05324> (2014).
21. Wang, Y. *et al.* Long-term cultured mesenchymal stem cells frequently develop genomic mutations but do not undergo malignant transformation. *Cell Death Dis* **4**, e950, <https://doi.org/10.1038/cddis.2013.480> (2013).
22. Lim, D. *et al.* Calcium homeostasis and mitochondrial dysfunction in striatal neurons of Huntington disease. *J Biol Chem* **283**, 5780–5789, <https://doi.org/10.1074/jbc.M704704200> (2008).
23. Acuna, A. I. *et al.* A failure in energy metabolism and antioxidant uptake precede symptoms of Huntington's disease in mice. *Nature communications* **4**, 2917, <https://doi.org/10.1038/ncomms3917> (2013).
24. Blazquez, C. *et al.* Loss of striatal type 1 cannabinoid receptors is a key pathogenic factor in Huntington's disease. *Brain* **134**, 119–136, <https://doi.org/10.1093/brain/awq278> (2011).
25. Lajoie, P. & Snapp, E. L. Changes in BiP availability reveal hypersensitivity to acute endoplasmic reticulum stress in cells expressing mutant huntingtin. *J Cell Sci* **124**, 3332–3343, <https://doi.org/10.1242/jcs.087510> (2011).
26. Chopra, V. *et al.* A small-molecule therapeutic lead for Huntington's disease: Preclinical pharmacology and efficacy of C2-8 in the R6/2 transgenic mouse. *Proceedings of the National Academy of Sciences* **104**, 16685–16689, <https://doi.org/10.1073/pnas.0707842104> (2007).
27. Levine, M. S. *et al.* Enhanced sensitivity to N-methyl-D-aspartate receptor activation in transgenic and knockin mouse models of Huntington's disease. *J Neurosci Res* **58**, 515–532 (1999).
28. Slow, E. J. *et al.* Selective striatal neuronal loss in a YAC128 mouse model of Huntington disease. *Human Molecular Genetics* **12**, 1555–1567, <https://doi.org/10.1093/hmg/ddg169> (2003).
29. Vonsattel, J. P. G., Keller, C. & Pilar Amaya, Md Neuropathology of Huntington's Disease. *Handbook of Clinical Neurology* **89**, 599–618 (2008).
30. Munsie, L. *et al.* Mutant huntingtin causes defective actin remodeling during stress: defining a new role for transglutaminase 2 in neurodegenerative disease. *Human Molecular Genetics* **20**, 1937–1951, <https://doi.org/10.1093/hmg/ddr075> (2011).
31. Godin, J. D. *et al.* Huntingtin Is Required for Mitotic Spindle Orientation and Mammalian Neurogenesis. *Neuron* **67**, 392–406, <https://doi.org/10.1016/j.neuron.2010.06.027>.
32. Molina-Calavita, M. *et al.* Mutant Huntingtin Affects Cortical Progenitor Cell Division and Development of the Mouse Neocortex. *The Journal of Neuroscience* **34**, 10034–10040, <https://doi.org/10.1523/jneurosci.0715-14.2014> (2014).
33. Ribeiro, M., Silva, A. C., Rodrigues, J., Naia, L. & Rego, A. C. Oxidizing effects of exogenous stressors in Huntington's disease knock-in striatal cells—protective effect of cystamine and creatine. *Toxicol Sci* **136**, 487–499, <https://doi.org/10.1093/toxsci/kft199> (2013).
34. Oliveira, A. M. *et al.* Protective effects of 3-alkyl luteolin derivatives are mediated by Nrf2 transcriptional activity and decreased oxidative stress in Huntington's disease mouse striatal cells. *Neurochemistry International* **91**, 1–12 (2015).
35. Ruiz, C. *et al.* Protection by glia-conditioned medium in a cell model of Huntington disease. *PLoS Currents* **4**, e4fbca54a2028b, <https://doi.org/10.1371/4fbca54a2028b> (2012).
36. Rigamonti, D. *et al.* Wild-type huntingtin protects from apoptosis upstream of caspase-3. *Journal of Neuroscience* **20**, 3705–3713 (2000).
37. Li, S.-H., Cheng, A. L., Li, H. & Li, X.-J. Cellular Defects and Altered Gene Expression in PC12 Cells Stably Expressing Mutant Huntingtin. *The Journal of Neuroscience* **19**, 5159–5172 (1999).
38. Dudek, H. *et al.* Regulation of Neuronal Survival by the Serine-Threonine Protein Kinase Akt. *Science* **275**, 661 (1997).
39. Geiger, T., Cox, J. & Mann, M. Proteomic changes resulting from gene copy number variations in cancer cells. *PLoS Genet* **6**, e1001090, <https://doi.org/10.1371/journal.pgen.1001090> (2010).
40. Stingle, S. *et al.* Global analysis of genome, transcriptome and proteome reveals the response to aneuploidy in human cells. *Mol Syst Biol* **8**, 608, <https://doi.org/10.1038/msb.2012.40> (2012).
41. Bae, B. I. *et al.* Mutant huntingtin: nuclear translocation and cytotoxicity mediated by GAPDH. *Proc Natl Acad Sci USA* **103**, 3405–3409, <https://doi.org/10.1073/pnas.0511316103> (2006).
42. Burke, J. R. *et al.* Huntingtin and DRPLA proteins selectively interact with the enzyme GAPDH. *Nat Med* **2**, 347–350 (1996).
43. Senatorov, V. V., Charles, V., Reddy, P. H., Tagle, D. A. & Chuang, D. M. Overexpression and nuclear accumulation of glyceraldehyde-3-phosphate dehydrogenase in a transgenic mouse model of Huntington's disease. *Mol Cell Neurosci* **22**, 285–297 (2003).
44. Eggers, S. & Sinclair, A. Mammalian sex determination—insights from humans and mice. *Chromosome Research* **20**, 215–238, <https://doi.org/10.1007/s10577-012-9274-3> (2012).
45. Ferrante, R. J. Mouse Models of Huntington's Disease and Methodological Considerations for Therapeutic Trials. *Biochimica et biophysica acta* **1792**, 506–520, <https://doi.org/10.1016/j.bbdis.2009.04.001> (2009).
46. Maiuri, T. *et al.* Huntingtin is a scaffolding protein in the ATM oxidative DNA damage response complex. *Human Molecular Genetics* **26**, 395–406, <https://doi.org/10.1093/hmg/ddw395> (2017).
47. von Horsten, S. *et al.* Transgenic rat model of Huntington's disease. *Hum Mol Genet* **12**, 617–624 (2003).
48. Mittelman, D. & Wilson, J. H. The fractured genome of HeLa cells. *Genome Biology* **14**, 111, <https://doi.org/10.1186/gb-2013-14-4-111> (2013).
49. Segawa, K., Minowa, A., Sugasawa, K., Takano, T. & Hanaoka, F. Abrogation of p53-mediated transactivation by SV40 large T antigen. *Oncogene* **8**, 543–548 (1993).
50. Ali, S. H. & DeCaprio, J. A. Cellular transformation by SV40 large T antigen: interaction with host proteins. *Seminars in Cancer Biology* **11**, 15–22, <https://doi.org/10.1006/scbi.2000.0342> (2001).
51. Feng, Z. *et al.* p53 tumor suppressor protein regulates the levels of huntingtin gene expression. *Oncogene* **25**, 1 (2006).
52. Bae, B. I. *et al.* p53 mediates cellular dysfunction and behavioral abnormalities in Huntington's disease. *Neuron* **47**, 29–41, <https://doi.org/10.1016/j.neuron.2005.06.005> (2005).
53. Abramoff, M. D. M., Paulo, J. & Ram, Sunanda, J. Image Processing with ImageJ. *Biophotonics International* (2004).
54. Eppig, J. T. *Rules for Nomenclature of Mouse Chromosome Aberrations*, <http://www.informatics.jax.org/mgihome/nomen/anomalies.shtml> (2015).

## Acknowledgements

J.J.W. was funded by the Baden-Wuerttemberg Foundation (research grant number P-BWS-SPII/3-08). The work was supported by the European Union 7th Framework Program (FP7/2012), Project “SWITCH-HD”, under grant agreement No. 324495 to H.P.N. L.E.C. was a postdoctoral fellow of the SWITCH-HD project. We are grateful to Alissa Mitnik and Tanja Wlodkowski for making the first cell size analyses in *STHdh* cells, Midea Ortiz Rios for supportive cell culture work and Eva Haydt for harvesting the different cultures for karyotyping as well as Jeannette Schoene for technical assistance.

### Author Contributions

L.E.C., C.W., J.J.W., O.R. and H.P.N. developed the conceptual framework for the study. E.S., C.W., A.-C.K. and L.E.C. performed cell size and proliferation analyses. U.A.M.-H. performed karyotyping. J.J.W. performed the analysis of protein markers. E.S., C.W., A.-C.K., N.R. and L.E.C. determined cell viability. L.E.C., C.W., J.J.W., E.S., U.A.M.-H., and H.P.N. interpreted the data. L.E.C., C.W., J.J.W. and E.S. prepared the Figures. L.E.C., E.S., C.W., J.J.W. and H.P.N. wrote the manuscript. All authors reviewed the manuscript.

### Additional Information

**Supplementary information** accompanies this paper at <https://doi.org/10.1038/s41598-017-17275-4>.

**Competing Interests:** The authors declare that they have no competing interests.

**Publisher's note:** Springer Nature remains neutral with regard to jurisdictional claims in published maps and institutional affiliations.



**Open Access** This article is licensed under a Creative Commons Attribution 4.0 International License, which permits use, sharing, adaptation, distribution and reproduction in any medium or format, as long as you give appropriate credit to the original author(s) and the source, provide a link to the Creative Commons license, and indicate if changes were made. The images or other third party material in this article are included in the article's Creative Commons license, unless indicated otherwise in a credit line to the material. If material is not included in the article's Creative Commons license and your intended use is not permitted by statutory regulation or exceeds the permitted use, you will need to obtain permission directly from the copyright holder. To view a copy of this license, visit <http://creativecommons.org/licenses/by/4.0/>.

© The Author(s) 2017